TiL_4-Coordinated Black Phosphorus Quantum Dots as an Efficient Contrast Agent for In Vivo Photoacoustic Imaging of Cancer

Zhengbo Sun, Yuetao Zhao, Zhibin Li, Haodong Cui, Yayan Zhou, Weihao Li, Wei Tao, Han Zhang, Huaiyu Wang,* Paul K. Chu, and Xue-Feng Yu**

Noninvasive cancer imaging has drawn research interest on account of the considerable benefits to patients by reducing unnecessary biopsies and facilitating imaging-guided therapy.[1] As one of the latest and promising biophotonic diagnostic modalities,[2] photoacoustic (PA) imaging has be shown to be more superior compared to many other traditional optical imaging techniques, for instance, high image contrast and sensitivity, high spatial resolution with depths up to several centimeters, and depth-resolved 3D imaging, thereby boding well for in vivo bioimaging.[3] Although the PA signal originates from the tumor site, the intensity is rather low especially in the early stage and therefore, an effective exogenous contrast agent is highly desirable for in vivo PA imaging of the tumor location.

Employment of inorganic nanomaterials as exogenous agents is of interest because their unique properties are better than those of organic molecules in in vivo PA bioimaging.[4] Since near-infrared (NIR) light can penetrate tissues, various NIR absorbing nanomaterials including metals, semiconductors, and carbon nanostructures have been explored.[5] Compared to organic dyes, inorganic nanoparticles can passively accumulate in tumors at larger concentration via the well-known enhanced permeability and retention (EPR) effect.[6] However, the potential long-term toxicity of the inorganic nanomaterials hamper wider adoption[7] and consequently, a new bioimaging nanoagent with good biocompatibility and efficient PA performance is demanded.

Atomically thin black phosphorus (BP) is a new member of 2D materials family. Different from other 2D materials such as graphene, BP has a layer-dependent bandgap between 0.3 and 2.0 eV and is more versatile in electronic and optoelectronic applications.[8] Recently, ultrasmall BP nanosheets (referred to as BP quantum dots, BPQDs) prepared by liquid exfoliation have been shown to have good biocompatiblity, photothermal performance, and nonlinear optical properties.[8f,9] Nevertheless, BP is very reactive to oxygen and water, resulting in compositional/physical changes as well as subsequent degradation in the optical properties[10] and bioapplications. In this study, by means of surface coordination,[11] a sulfonic ester of the titanium ligand (TiL_4) is coordinated with the BPQDs to improve the stability in aqueous dispersions and the use of the materials as a photoacoustic imaging (PAI) agent in in vivo bioimaging of cancer is evaluated.

The TiL_4, a titanium sulfonate ligand (Figure S1a, Supporting Information), is synthesized by reacting titanium tetraisopropoxide [$Ti(OiPr)_4$] with *p*-toluenesulfonic acid in ethanol.[11] The BPQDs prepared by a liquid exfoliation technique[8f] are mixed with TiL_4 in *N*-methyl-2-pyrrolidone (NMP) at room temperature for 15 h to generate TiL_4@BPQDs (Figure S1b, Supporting Information). Transmission electron microscopy (TEM) and atomic force microscopy (AFM) are performed to examine the morphology of the TiL_4@BPQDs. The TEM images in **Figure 1**a and Figure S2 (Supporting Information) reveal the ultrasmall TiL_4@BPQDs and the high-resolution TEM (HR-TEM) image in the inset shows lattice fringes of 0.34 nm ascribed to the (021) plane of the BP crystal. The topographical AFM image in Figure 1c shows that the measured heights of the TiL_4@BPQDs are 1.6, 2.1, and 2.2 nm,

Dr. Z. Sun, W. Tao, Prof. H. Zhang
Shenzhen Key Laboratory of Two-Dimensional Materials and Devices (SKTMD)
SZU-NUS Collaborative Innovation Center for Optoelectronic Science and Technology
Key Laboratory of Optoelectronic Devices and Systems of Ministry of Education and Guangdong Province
College of Optoelectronic Engineering
Shenzhen University
Shenzhen 518060, P. R. China
E-mail: hzhang@szu.edu.cn

Dr. Z. Sun, Y. Zhao, H. Cui, Prof. H. Wang, Prof. X.-F. Yu
Institute of Biomedicine and Biotechnology
Shenzhen Institutes of Advanced Technology
Chinese Academy of Sciences
Shenzhen 518055, P. R. China
E-mail: hywang1@siat.ac.cn; xf.yu@siat.ac.cn

Dr. Z. Li, Prof. P. K. Chu
Department of Physics and Materials Science
City University of Hong Kong
Tat Chee Avenue, Kowloon, Hong Kong 99077, China

Dr. Y. Zhou, W. Li
Department of Radiation Therapy
Shenzhen People's Hospital
2nd Clinical Medical Collage of Jinan University
Shenzhen, Guangdong 518055, P. R. China

DOI: 10.1002/smll.201602896

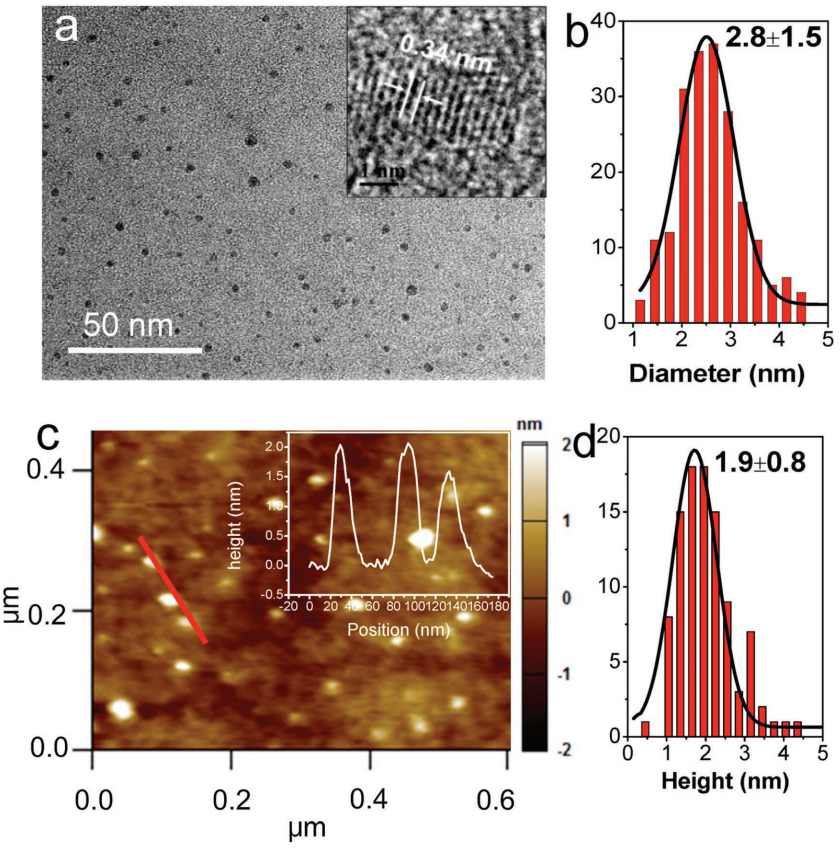

Figure 1. Synthesis and characterization of TiL_4@BPQDs. a) TEM image and HR-TEM image (inset). b) Statistical analysis of the lateral size of the 100 TiL_4@BPQDs based on TEM. c) AFM image and height profiles along the red line. d) Statistical analysis of the heights of 100 TiL_4@ BPQDs according to AFM.

respectively. According to the statistical TEM and AFM analysis of 100 TiL_4@BPQDs (Figure 1c,d), the lateral size of the TiL_4@BPQDs is 2.8 ± 1.5 nm and the thickness is 2.0 ± 0.6 nm. Raman scattering is conducted and Figure S3 (Supporting Information) shows three prominent peaks, the out-of-plane phonon mode (A^1_g) at 359.5 cm^{-1} as well as two in-plane modes, B_{2g} and A^2_g, at 436.0 and 463.3 cm^{-1}, respectively. Compared to bulk BP, the A^1_g, B_{2g}, and A^2_g modes of the TiL_4@BPQDs red-shift by about 1.3, 2.4, and 1.7 cm^{-1}, respectively, which are similar to those observed from few-layer BP nanosheets.

The TiL_4@BPQDs supernatants with different concentrations are characterized by ultraviolet–visible–near infrared (UV–vis–NIR) absorption spectroscopy (**Figure 2**a). The optical absorption spectra acquired from the TiL_4@BPQDs disclose a broad absorption band spanning the UV and NIR regions similar to BPQDs.[11] The normalized absorption intensity over the characteristic cell length (A/L) at $\lambda = 680$ nm is determined (see Figure 2b) at different concentrations (C) and the amount of TiL_4@BPQDs is determined by inductively coupled plasma atomic-emission spectroscopy (ICP-AES). According to the Lambert–Beer law: $A/L = \alpha C$, where A is the absorbance intensity, L is the cell length, α is the extinction coefficient, and C is the concentration, a linear trend is observed for the A/L versus concentration relationship and the extinction coefficient at 680 nm is calculated to be 22.2 L g^{-1} cm^{-1}.

To evaluate the stability of BPQDs after TiL_4 surface coordination, the bare BPQDs and TiL_4@BPQDs are centrifuged from NMP, resuspended in water at the same concentration, and then exposed to ambient air for 10 d. As shown in Figure 2c, both the bare BP and TiL_4@BPQDs solutions are brown in the beginning after resuspension, but only the bare BP solution fades in color becoming more clear and transparent after 10 d. The corresponding absorbance intensity decreases significantly with storage time (Figure 2d) and after 10 d, the absorbance of the bare BP solution at 450 nm (A) decreases to 43% of the original value (A_0). In comparison, the absorbance of the TiL_4@BP solution only decreases by about 10%. Furthermore, the two samples are dispersed in the medium comprised of Dulbecco's Modified Eagle Medium (DMEM) and 10% fetal bovine serum (FBS) for 10 d to examine their stability in biological environment. In line with the results shown in Figure 2c,d, both BPQDs and TiL_4@BPQDs are nonaggregating in the medium but only the TiL_4@BPQDs exhibit a good stability (Figure S4, Supporting Information). It has been expounded that the degradation of BP is initiated by the oxidation reaction, in which the lone pair electrons of BP can be readily occupied by the ambient oxygen to form P_xO_y.[7j] While the lone pair electrons of BP are deprived by the electrophilic TiL_4, the reaction between BP and the ambient oxygen can be efficiently prevented.[11] Our results produce evidence that TiL_4 coordination enhances the stability of the BPQDs.

Light between 650 and 950 nm is usually referred to as the "NIR optical window" and promising is biomedical imaging and detection because the radiation provides deeper tissue penetration and reduced photodamage. The performance of the TiL_4@BPQDs is further studied at different NIR wavelengths as shown in **Figure 3**. The PA signal intensity decreases as the laser wavelength is increased from 680 to 808 nm. When an optical absorbing material such as BPQDs is irradiated by laser pulses shorter than the thermal transport time of the absorbed energy, transient thermoelastic expansion occurs and a subsequent PA pressure wave is generated.[12] During the thermal expansion in an optical absorber, the conversion efficiency of light energy to PA pressure wave plays a key role in the PA signal generation. The conversion efficiency is mainly determined by the light absorbance and heat capacity of the optical absorber. Therefore, the PA signal intensity of the TiL_4@BPQDs diminishes with decreasing optical absorption from 680 to 808 nm. Our data also suggest that the optimal signal occurs at the wavelength of 680 nm which is used in our subsequent experiments.

The PA performance of the TiL_4@BPQDs is further evaluated by comparing them with those of Au nanorods

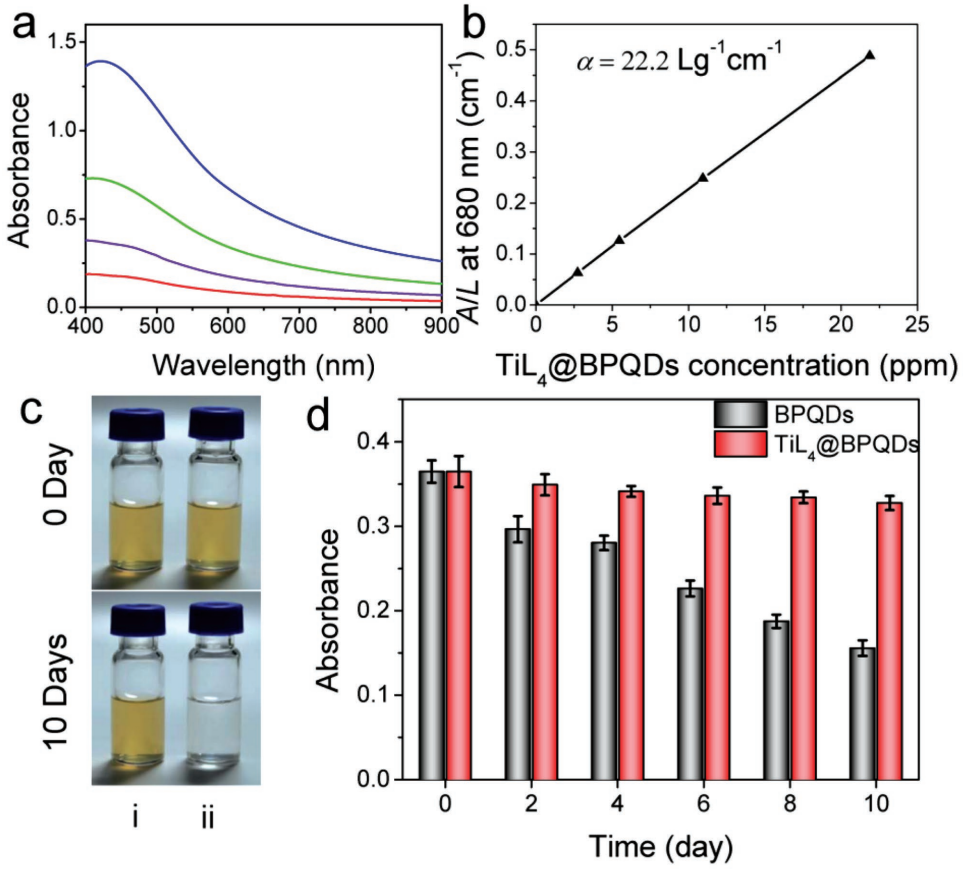

Figure 2. Optical properties and stability of TiL_4@ BPQDs. a) Absorbance spectra of TiL_4@BPQDs dispersed in water at different concentrations. The top curve is obtained from the TiL_4@ BPQDs solution at 22.0 ppm and each subsequent curve represents the TiL_4@ BPQDs solution after two times dilution. b) Normalized absorbance intensity over the characteristic cell length (A/L) at different concentrations for $\lambda = 680$ nm. c) Photographs of (i) BPQDs and (ii) TiL_4@BPQDs (ii) dispersed in water after 0 and 10 d, respectively. d) Absorbance (450 nm) of BPQDs and TiL_4@ BPQDs with dispersion time in water.

(AuNRs) which have been studied as PA contrast agents.[50] The solutions containing 22.0 ppm of TiL_4@BPQDs or 79.8 ppm of AuNRs are prepared to achieve optical densities of 0.50 at 680 nm (Figure S5, Supporting Information). Afterward, the TiL_4@BPQDs and AuNRs solutions are twice-diluted four times with the optical densities at 680 nm varying from 0.500 to 0.031, placed in a tomographic scanner, and imaged with 680 nm light excitation. **Figure 4**a shows the concentration-dependent PA signals of the TiL_4@BPQDs and AuNRs solutions. It is clear that the TiL_4@BPQDs performs better than the AuNRs at the same concentration. The corresponding PA signal intensities of the TiL_4@BPQDs and AuNRs are presented in Figure 4b which shows that the PA signal of the TiL_4@BPQDs is nearly 7.29 times that of the AuNRs when the optical densities of both samples are 0.50 at 680 nm. Even at 730 nm wavelength, which is close to the peak of the absorption spectrum of the AuNRs, the PA signal intensity of AuNRs is still much weaker than that of TiL_4@ BPQDs (Figure S6, Supporting Information). The calculated limit of detection of TiL_4@BPQDs is as small as 0.125 (corresponding to only 5.5 ppm), demonstrating the excellent performance of the TiL_4@BPQDs as a PA agent.

After the demonstration of good cytocompatibilty (Figure S7, Supporting Information), the TiL_4@BPQDs are further evaluated for their PA sensitivity in vitro (see **Figure 5**). The MCF-7 cancer cells are incubated with TiL_4@ BPQDs at different concentrations (0, 6.25, 12.5, 25, 50, and 100 ppm) before 680 nm PA examination. The PA images and corresponding quantitative intensity analysis are shown in Figure 5a. The cells after TiL_4@BPQDs addition are significant and the disturbance from endogenous absorbers is negligible in the biological system. The PA signal increases with the amount of TiL_4@BPQDs. An obvious PA signal can be observed from the cells after addition of only 12.5 ppm of TiL_4@BPQDs (only 0.63% of the common imaging dose of 2 mg L^{-1}), suggesting the high sensitivity in in vitro PA imaging. The PA performance for different cell numbers (0.16, 0.32, 0.63, 1.25, 2.5, and 5.0 million) is examined after the addition of 50 ppm of TiL_4@BPQDs. As shown in Figure 5b, the cell PA signal stands out from the background even though the cell number is only 0.63 million. Since there are around 10^8 cells in 1 cm^3 of tumor,[13] the high PA sensitivity of TiL_4@BPQDs with the detection limit at least of 0.63 million cancer cells indicates that this agent can detect very small lesions.

In vivo PA imaging experiments are performed with the TiL_4@BPQDs as the contrast agent. Eight-week-old nude male mice (Balb/C-nude) are injected with 8 million MCF-7

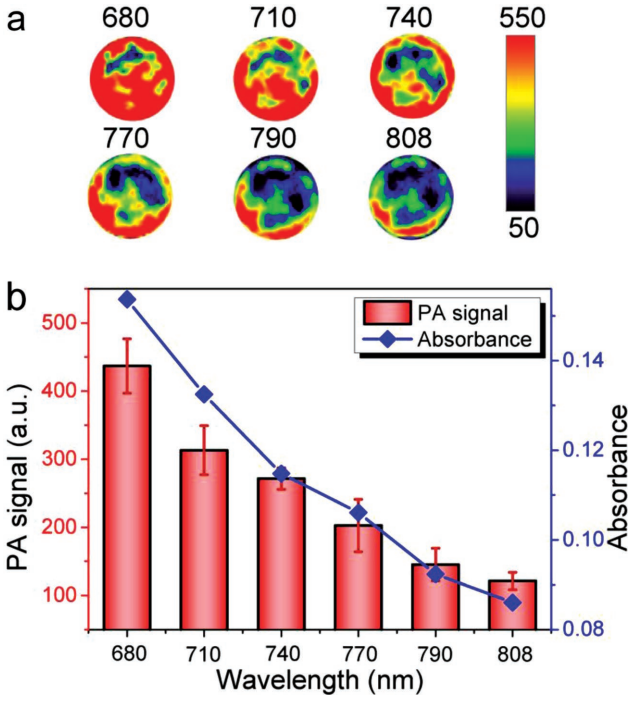

Figure 3. PA performance of TiL_4@ BPQDs at different wavelengths. a) PA images of TiL_4@BPQDs at different excitation wavelengths (680, 710, 740, 770, 790, and 808 nm). b) PA signal and corresponding absorption intensities of TiL_4@ BPQDs at different excitation wavelengths.

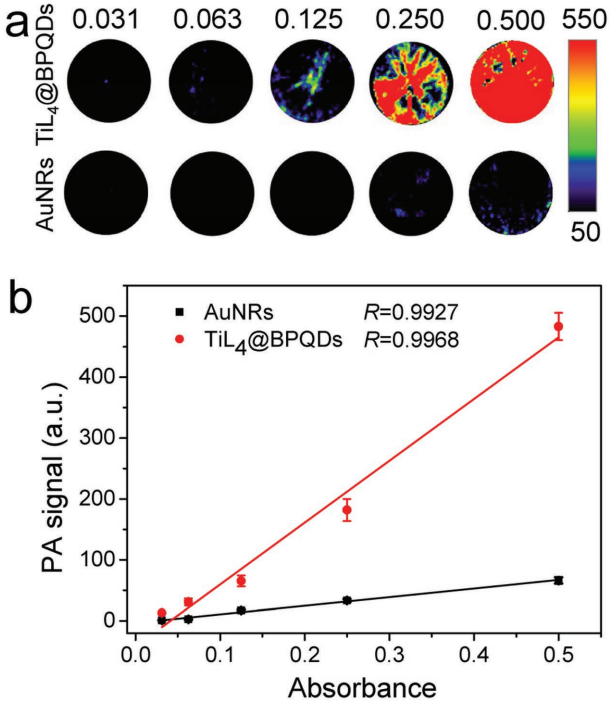

Figure 4. Comparison of PA performances between TiL_4@BPQDs and AuNRs. a) PA images of the TiL_4@BPQDs and AuNRs for different optical densities at 680 nm (0.031, 0.063, 0.125, 0.250, and 0.500). b) Corresponding signal intensities of the TiL_4@BPQDs and AuNRs for different optical densities at 680 nm (0.031, 0.063, 0.125, 0.250, and 0.500). For both samples, the PA intensity varies linearly with the optical density.

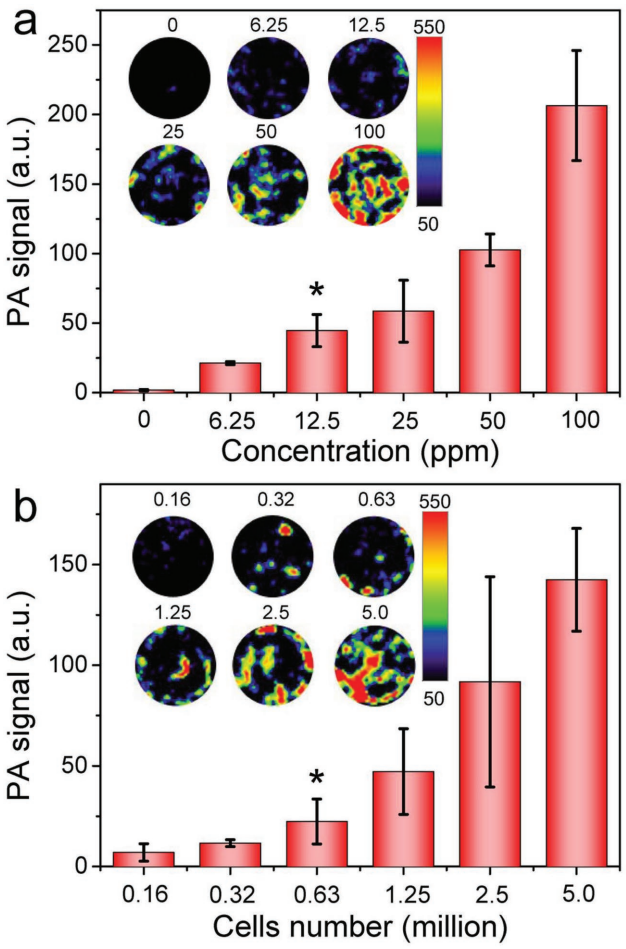

Figure 5. Cell detection sensitivity of TiL_4@BPQDs. a) PA images and corresponding quantitative intensity analysis of MCF-7 cells added with different amounts of TiL_4@BPQDs (6.25, 12.5, 25, 50, and 100 ppm). b) PA images and corresponding quantitative intensity analysis of different amounts of MCF-7 cells (0.16, 0.32, 0.63, 1.25, 2.5, and 5.0 million) added with 50 ppm of TiL_4@BPQDs. * means $p < 0.05$, compared to the control group.

cells through the rear leg flank. After intravenous injection of 200 μg of TiL_4@BPQDs, the mice bearing 0.5 to 0.7 cm^3 MCF-7 tumors are photoacoustically imaged on a commercial PA computed tomography system. The transverse slices of the host mice are formed by averaging the PA signals acquired from five laser pulses at 608 nm with 15 nm step intervals. PA imaging is performed prior to injection of the TiL_4@BPQDs at 0.5, 1, 2, 4, 6, 24, and 48 h postinjection. As shown in **Figure 6**a, some noisy PA signals in the skin area are detected from the preinjection group because of scattering by skin or the relative rigid effect during the change from transmission the gel to tissue. After injection of TiL_4@BPQDs, the mice show larger PA signals in the tumors than preinjection and the maximum is observed at 4 h postinjection. Afterward, the PA signal decreases gradually and returns to the low level similar to preinjection at 48 h postinjection. The contrast enhancement of the PA signal intensity in the region of interest (ROI) in the tumor site is plotted as a function of time after injection of TiL_4@BPQDs. As shown in Figure 6b, at preinjection and after 48 h postinjection, the

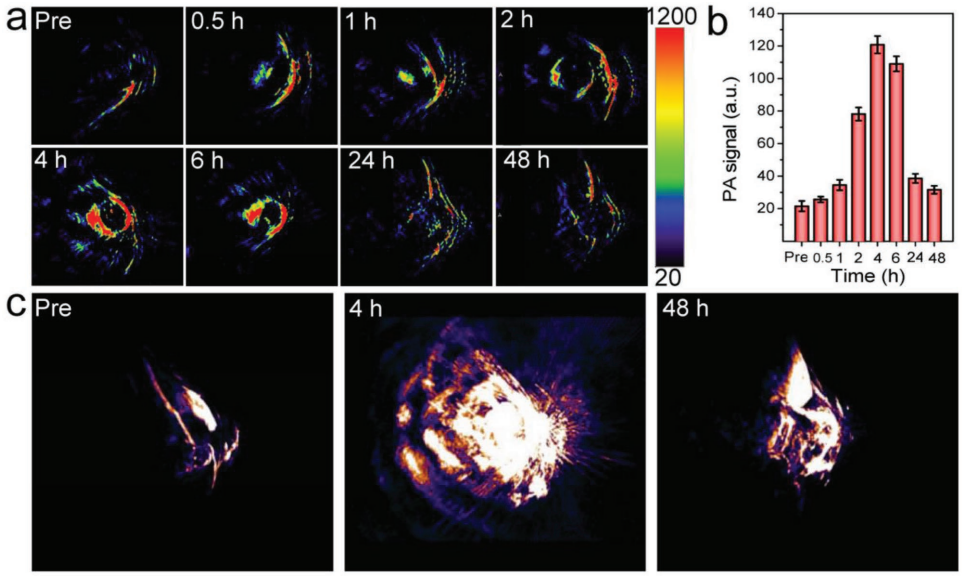

Figure 6. In vivo PA performances of TiL_4@BPQDs. a) Time-dependent PA images of the MCF-7 cells in the xenografted tumor in the BALB/c nude mice after intravenous injection of TiL_4@BPQDs. The signal intensity bar is shown on the right side. b) Quantitative analysis of each ROI signal in (a). c) Typical 3D PA images of the tumor at different time points pre- and postinjection of TiL_4@BPQDs.

PA signal intensities in the tumor area are 21.49 ± 3.16 and 31.58 ± 2.42 a.u., respectively. At 4 h postinjection, strong PA signals as high as 120.80 ± 5.40 a.u. can be observed from the tumor. The 3D PA images of the tumor site are acquired by using an Inveon research workplace (see Figure 6c) and a video clip of these multiple adjacent 2D image slices within the 3D image set is shown in Video M1-3 in the Supporting Information. The 3D images reveal that the PA signals in the tumor are significantly enhanced after TiL_4@BPQDs injection. The PA imaging demonstrate that the TiL_4@BPQDs after intravenous administration can accumulate in the tumor, which probably due to the following points. First, it is measured that the zeta potential of BPQDs is changed from –36.5 ± 1.1 to +21.1 ± 2.56 mV after TiL_4-coordination. Since tumor cell membrane generally covers with numerous negatively charge, the positively charged TiL_4@BPQDs can enhance tumor cell targeting and cellular internalization.[14] Second, further dynamic light scattering (DLS) measurement reveals that the hydrodynamic size of TiL_4@BPQDs is about 275.0 ± 55 nm in culture medium comprised of DMEM and 10% FBS (Figure S8, Supporting Information), and the nanoparticles with hydrodynamic size larger than 50 nm are more efficient to escape rapid kidney filtration and passively accumulate in tumors via the EPR effect.[6] As before mentioned, the TiL_4@BPQDs are in the size of only several nanometers under TEM observation (Figure 1). The size differentiation measured by DLS and TEM can be attributed to the different measurement conditions.[15] The TiL_4@BPQDs are dispersed in culture medium for DLS determination but they should be vacuum-dried for TEM examination. Because of their positive charge and high surface energy of nanoparticles, once the TiL_4@BPQDs are introduced into culture medium, many negatively charged proteins could interact with the particle surface and form the "protein corona," and resulting in a dramatic increase in their hydrodynamic size.[16]

In summary, TiL_4 coordinated BPQDs are prepared and demonstrated as efficient PA agents in bioimaging of cancer. Compared with bare BPQDs, the TiL_4@BPQDs exhibit enhanced stability in water dispersions. Owing to the large NIR extinction coefficient, the TiL_4@BPQDs exhibit excellent PA performance at 680 nm superior to that of AuNRs. Our in vitro and in vivo experiments further demonstrate the excellent sensitivity and high spatial resolution in detecting tumors clearly, demonstrating the large potential of the TiL_4@BPQDs in clinical applications.

Experimental Section

Materials: The BP crystals were purchased from a commercial supplier (Smart-Elements) and stored in a dark Ar glovebox. The NMP (99.5%, anhydrous) was purchased from Aladdin. phosphate buffer saline (PBS) (pH 7.4) and FBS, DMEM, trypsin-EDTA, and penicillin–streptomycin were purchased from Gibco Life Technologies (AG, Switzerland). Dimethyl Sulphoxide (DMSO) was obtained from Sinopharm Chemical Reagent Co., Ltd. (Shanghai, China). All other chemicals used in this study were analytical reagent grade and used without further purification. Ultrapure water (18.25 MΩ cm, 25 °C) was used to prepare the solutions.

Synthesis of TiL4@BPQDs: The TiL_4@BPQDs were synthesized by the method reported by our group previously.[11] In brief, 25 mg of the BP powder was added to 25 mL of NMP in a 50 mL sealed conical tube and sonicated with a sonic tip for 3 h at 1200 W, ultrasonic frequencies from 19 to 25 kHz, and ultrasound probe time of 2 s at an interval of 4 s. The dispersion was sonicated in an ultrasonic bath continuously for another 10 h at 300 W. The temperature of the solution was kept below 277 K in an ice bath. The dispersion was centrifuged for 20 min at 7000 rpm and the supernatant containing the BPQDs was decanted gently. The supernatant solution was centrifuged for 20 min at 12 000 rpm.

The precipitate was rinsed with water repeatedly and resuspended in the aqueous solution finally.

To achieve TiL_4 surface coordination, a proper amount of the synthesized TiL_4 was added to the BP (ultrasmall BP nanosheets and micrometer-sized BP sheets) solution in NMP (1 mL, 3.7 μmol) and the mixture was stirred in darkness under nitrogen for 15 h. The mixture was centrifuged at 12 000 rpm for 20 min and the precipitated TiL_4@BP was collected for use for subsequent experiments.

Characterization: The TEM and HR-TEM images were acquired on the Tecnai G2 F20 S-Twin transmission electron microscope at an acceleration voltage of 200 kV. AFM was performed on the drop-cast flakes on the Si/SiO_2 substrates using an MFP-3D-S atomic force microscopy (Asylum Research, USA) under the AC mode (tapping mode) in air. Zeta potentials were measured on a Zetasizer Nano ZS zeta analyzer. Raman scattering was performed on a Horiba Jobin-Yvon Lab Ram HR VIS high-resolution confocal Raman microscope equipped with a 633 nm laser as the excitation source at room temperature. The BP concentration was determined by ICP-AES (7000DV, PerkinElmer). The UV–vis–NIR absorption spectra were recorded on a Lambda25 spectrophotometer (PerkinElmer) with QS-grade quartz cuvettes at room temperature. The optical absorbance per cell length (A/L) was determined from the optical absorbance intensity at 808 nm. Using Beer's law ($A/L = \alpha C$), the BP extinction coefficient was extracted from the slope of a plot of A/L versus concentration.

Evaluation of In Vitro PA Imaging: In in vitro PA imaging, the solutions containing different amounts of TiL_4@BPQDs dissolved in PBS were placed in a hemispherical acrylic holder and suspended in the center of the imaging dimple of the Nexus 128 PA instrument (Endra Life Sciences). The transducers were coupled to the sample plane by filling the bowl with water and maintained at 38 °C by a pumping system. Six sets of PA signal data were acquired at incident laser wavelengths of 680, 710, 740, 770, 790, and 808 nm. The PA signal intensities were analyzed using the ROI in the baseline image and the intensity changes in the ROI of the five images were calculated. The solutions containing TiL_4@BPQDs and AuNRs with different absorbance values of 0.031, 0.063, 0.125, 0.250, and 0.500 were placed directly in the imaging dimple and the PA signal detected at 680 nm.

Cellular Toxicity Assay: The 293T human embryonic kidney cells and MCF-7 breast cancer cells were obtained from China type culture collection (CTCC). These cells were cultured on a 96-well plate (1×10^4 cells per well) in Dulbecco's modified Eagle medium (Gibco BRL) supplemented with 10% (v/v) fetal bovine serum, supplemented with 100 UI mL^{-1} penicillin and 100 UI mL^{-1} streptomycin, in a humid chamber of 5% CO_2 at 37 °C. After 12 h of initial cell culture, the medium was refreshed with 200 μL of culture media containing BPQDs and TiL_4@BPQDs at different concentrations (25, 50, 100, and 200 ppm). After 48 h of coincubation, the cells were washed twice with PBS then 10 μL of CCK-8 solution was added onto each well and incubated for another 2 h at 37 °C. The absorbance was measured at a wavelength of 450 nm by using a microplate reader (Varioskan Flash 4.00.53, Finland). The cell viability was normalized to the control group and the following formula was used to evaluate cell viability: Cell viability (%) = (mean of Abs. value of treatment group/mean Abs. value of control) × 100%. For each kind of samples, the cell viability assay was performed in quintuplicate.

PA Imaging of Intracellular TiL_4@BPQDs: The MCF-7 cells were obtained from CTCC. The cells were cultured on a 6-wells plate (1×10^4 cells per well) in Dulbecco's modified Eagle medium (Gibco BRL) supplemented with 10% (v/v) fetal bovine serum supplemented with 100 UI mL^{-1} penicillin and 100 UI mL^{-1} streptomycin. The cells were incubated in a humid chamber of 5% CO_2 at 37 °C. After incubation for 24 h, the cell media in the wells were replaced with either fresh medium (no nanoparticles) or new culture medium containing different amounts (6.25, 12.5, 25, 50, and 100 ppm) of TiL_4@BPQDs. After incubation for 4 h, the cells were treated with trypsin–EDTA solution, harvested into a 1.5 mL conical tube, and centrifuged (600 g, 3 min) to produce a cell pellet. The supernatant was gently replaced with fresh PBS. The samples were investigated by PA imaging. The solutions were placed directly in the imaging dimple and PA signal was acquired at 680 nm.

Different amounts of MCF-7 cells (0.16, 0.32, 0.63, 1.25, 2.5, and 5.0 million) were incubated in the culture medium containing 50 ppm of TiL_4@BPQDs for 2 h at 37 °C. After washing three times with cold PBS, the cells were suspended in 50 μL PBS and placed directly in the dimple of the PA instrument for determination of PA signal. All the experiments were performed in triplicates.

PA Imaging of TiL_4@BPQDs in MCF-7 Tumors in Mice: The animal studies were performed in accordance with the Guidelines for the Care and Use of Research Animals established by the Stanford University (Stanford, CA). Eight-week-old nude male mice (Balb/C-nude) were injected with 8 million MCF-7 cells via the rear leg flank. The mice bearing 0.5 to 0.7 cm^3 MCF-7 tumors were photoacoustically imaged on a commercial PA computed tomography system (Nexus 128, Endra Inc.). The system used a tunable nanosecond pulsed laser (7 ns pulses, 20 Hz pulse repetition frequency, about 7 mJ per pulse on the animal surface, wavelength range 680 to 950 nm) and 128 unfocused ultrasound transducers (with 5 MHz center frequency and 3 mm diameter) arranged in a hemispherical bowl filled with water. We used 680 nm light with 20 views and 30 pulses per view. For each animal, we first obtained preinjection data at 680 nm. The imaging agent (200 μg) was dissolved in 100 μL PBS (pH 7.4) and administered to the mice by tail-vein injection. The data were acquired at 0.5, 1, 2, 4, 6, 24, and 48 h after injection of the imaging agent. The volume rendered 3D PA images were reconstructed off-line using data acquired from all 128 transducers from all views using a filtered back-projection algorithm. The algorithm corrected for pulse-to-pulse variations in the laser intensity and small changes in the temperature that affected the acoustic velocity in the water. The reconstructed 3D raw data were then analyzed using Osirix software.

Supporting Information

Supporting Information is available from the Wiley Online Library or from the author.

Acknowledgements

This work was supported by the NSFC (51672305, 81501577, 61435010, and 61222505), Science and Technology Key Project of

Shenzhen (JCY20160229195124187, JCYJ20150403102020235, and KQTD2015032416270385), Frontier Research Key Project of the Chinese Academy of Sciences (QYZDB-SSW-SLH034), China Postdoctoral Science Foundation (2015M570725), Hong Kong Research Grants Council (RGC) General Research Funds No. CityU 11301215, and Hong Kong Scholars Program.

[1] S. Kunjachan, J. Ehling, G. Storm, F. Kiessling, T. Lammers, *Chem. Rev.* **2015**, *115*, 10907.
[2] L. H. V. Wang, S. Hu, *Science* **2012**, *335*, 1458.
[3] X. D. Wang, Y. J. Pang, G. Ku, X. Y. Xie, G. Stoica, L. H. V. Wang, *Nat. Biotechnol.* **2003**, *21*, 803.
[4] A. P. Jathoul, J. Laufer, O. Ogunlade, B. Treeby, B. Cox, E. Zhang, P. Johnson, A. R. Pizzey, B. Philip, T. Marafioti, M. F. Lythgoe, R. B. Pedley, M. A. Pule, P. Beard, *Nat. Photonics* **2015**, *9*, 239.
[5] a) G. P. Luke, D. Yeager, S. Y. Emelianov, *Ann. Biomed. Eng.* **2012**, *40*, 422; b) M. F. Kircher, A. de la Zerda, J. V. Jokerst, C. L. Zavaleta, P. J. Kempen, E. Mittra, K. Pitter, R. M. Huang, C. Campos, F. Habte, R. Sinclair, C. W. Brennan, I. K. Mellinghoff, E. C. Holland, S. S. Gambhir, *Nat. Med.* **2012**, *18*, 829; c) A. de la Zerda, S. Bodapati, R. Teed, S. Y. May, S. M. Tabakman, Z. Liu, B. T. Khuri-Yakub, X. Y. Chen, H. J. Dai, S. S. Gambhir, *ACS Nano* **2012**, *6*, 4694; d) A. De La Zerda, C. Zavaleta, S. Keren, S. Vaithilingam, S. Bodapati, Z. Liu, J. Levi, B. R. Smith, T. J. Ma, O. Oralkan, Z. Cheng, X. Y. Chen, H. J. Dai, B. T. Khuri-Yakub, S. S. Gambhir, *Nat. Nanotechnol.* **2008**, *3*, 557; e) H. W. Yang, H. L. Liu, M. L. Li, I. W. Hsi, C. T. Fan, C. Y. Huang, Y. J. Lu, M. Y. Hua, H. Y. Chou, J. W. Liaw, C. C. M. Ma, K. C. Wei, *Biomaterials* **2013**, *34*, 5651; f) L. M. Nie, S. J. Wang, X. Y. Wang, P. F. Rong, A. Bhirde, Y. Ma, G. Liu, P. Huang, G. M. Lu, X. Y. Chen, *Small* **2014**, *10*, 1585; g) Z. H. Sheng, L. Song, J. X. Zheng, D. H. Hu, M. He, M. B. Zheng, G. H. Gao, P. Gong, P. F. Zhang, Y. F. Ma, L. T. Cai, *Biomaterials* **2013**, *34*, 5236; h) L. J. Jing, X. L. Liang, Z. J. Deng, S. S. Feng, X. D. Li, M. M. Huang, C. H. Li, Z. F. Dai, *Biomaterials* **2014**, *35*, 5814; i) W. W. Li, P. F. Rong, K. Yang, P. Huang, K. Sun, X. Y. Chen, *Biomaterials* **2015**, *45*, 18; j) X. Liu, W. C. Law, M. Jeon, X. L. Wang, M. X. Liu, C. Kim, P. N. Prasad, M. T. Swihart, *Adv. Healthcare Mater.* **2013**, *2*, 952; k) Y. Yong, X. J. Cheng, T. Bao, M. Zu, L. Yan, W. Y. Yin, C. C. Ge, D. L. Wang, Z. J. Gu, Y. L. Zhao, *ACS Nano* **2015**, *9*, 12451; l) U. S. Dinish, Z. G. Song, C. J. H. Ho, G. Balasundaram, A. B. E. Attia, X. M. Lu, B. Z. Tang, B. Liu, M. Olivo, *Adv. Funct. Mater.* **2015**, *25*, 2316; m) S. K. Maji, S. Sreejith, J. Joseph, M. J. Lin, T. C. He, Y. Tong, H. D. Sun, S. W. K. Yu, Y. L. Zhao, *Adv. Mater.* **2014**, *26*, 5633; n) X. L. Liang, Y. Y. Li, X. D. Li, L. J. Jing, Z. J. Deng, X. L. Yue, C. H. Li, Z. F. Dai, *Adv. Funct. Mater.* **2015**, *25*, 1451; o) J. V. Jokerst, A. J. Cole, D. Van de Sompel, S. S. Gambhir, *ACS Nano* **2012**, *6*, 10366; p) J. Liu, X. P. Zheng, L. Yan, L. J. Zhou, G. Tian, W. Y. Yin, L. M. Wang, Y. Liu, Z. B. Hu, Z. J. Gu, C. Y. Chen, Y. L. Zhao, *ACS Nano* **2015**, *9*, 696; q) L. Cheng, J. J. Liu, X. Gu, H. Gong, X. Z. Shi, T. Liu, C. Wang, X. Y. Wang, G. Liu, H. Y. Xing, W. B. Bu, B. Q. Sun, Z. Liu, *Adv. Mater.* **2014**, *26*, 1886; r) S. Mallidi, T. Larson, J. Tam, P. P. Joshi, A. Karpiouk, K. Sokolov, S. Emelianov, *Nano Lett.* **2009**, *9*, 2825; s) G. S. Song, J. L. Hao, C. Liang, T. Liu, M. Gao, L. Cheng, J. Q. Hu, Z. Liu, *Angew. Chem. Int. Ed.* **2016**, *55*, 2122.
[6] a) K. Yang, L. Z. Feng, X. Z. Shi, Z. Liu, *Chem. Soc. Rev.* **2013**, *42*, 530; b) L. R. Guo, I. Panderi, D. D. Yan, K. Szulak, Y. J. Li, Y. T. Chen, H. Ma, D. B. Niesen, N. Seeram, A. Ahmed, B. F. Yan, D. Pantazatos, W. Lu, *ACS Nano* **2013**, *7*, 8780.
[7] a) H. O. Churchill, P. Jarillo-Herrero, *Nat. Nanotechnol.* **2014**, *9*, 330; b) L. Li, Y. Yu, G. J. Ye, Q. Ge, X. Ou, H. Wu, D. Feng, X. H. Chen, Y. Zhang, *Nat. Nanotechnol.* **2014**, *9*, 372; c) H. Liu, A. T. Neal, Z. Zhu, Z. Luo, X. F. Xu, D. Tomanek, P. D. D. Ye, *ACS Nano* **2014**, *8*, 4033; d) J. S. Qiao, X. H. Kong, Z. X. Hu, F. Yang, W. Ji, *Nat. Commun.* **2014**, *5*, 4475; e) D. Xiang, C. Han, J. Wu, S. Zhong, Y. Y. Liu, J. D. Lin, X. A. Zhang, W. P. Hu, B. Ozyilmaz, A. H. C. Neto, A. T. S. Wee, W. Chen, *Nat. Commun.* **2015**, *6*, 6485; f) X. M. Wang, A. M. Jones, K. L. Seyler, V. Tran, Y. C. Jia, H. Zhao, H. Wang, L. Yang, X. D. Xu, F. N. Xia, *Nat. Nanotechnol.* **2015**, *10*, 517; g) J. X. Wu, N. N. Mao, L. M. Xie, H. Xu, J. Zhang, *Angew. Chem. Int. Ed.* **2015**, *54*, 2366; h) J. Sun, H. W. Lee, M. Pasta, H. T. Yuan, G. Y. Zheng, Y. M. Sun, Y. Z. Li, Y. Cui, *Nat. Nanotechnol.* **2015**, *10*, 980–U184-; i) S. Zhang, J. Yang, R. J. Xu, F. Wang, W. F. Li, M. Ghufran, Y. W. Zhang, Z. F. Yu, G. Zhang, Q. H. Qin, Y. R. Lu, *ACS Nano* **2014**, *8*, 9590; j) A. Favron, E. Gaufres, F. Fossard, A. L. Phaneuf-L'Heureux, N. Y. W. Tang, P. L. Levesque, A. Loiseau, R. Leonelli, S. Francoeur, R. Martel, *Nat. Mater.* **2015**, *14*, 826.
[8] a) J. R. Brent, N. Savjani, E. A. Lewis, S. J. Haigh, D. J. Lewis, P. O'Brien, *Chem. Commun.* **2014**, *50*, 13338; b) P. Yasaei, B. Kumar, T. Foroozan, C. H. Wang, M. Asadi, D. Tuschel, J. E. Indacochea, R. F. Klie, A. Salehi-Khojin, *Adv. Mater.* **2015**, *27*, 1887; c) X. Zhang, H. M. Xie, Z. D. Liu, C. L. Tan, Z. M. Luo, H. Li, J. D. Lin, L. Q. Sun, W. Chen, Z. C. Xu, L. H. Xie, W. Huang, H. Zhang, *Angew. Chem. Int. Ed.* **2015**, *54*, 3653; d) J. Kang, J. D. Wood, S. A. Wells, J. H. Lee, X. L. Liu, K. S. Chen, M. C. Hersam, *ACS Nano* **2015**, *9*, 3596; e) A. H. Woomer, T. W. Farnsworth, J. Hu, R. A. Wells, C. L. Donley, S. C. Warren, *ACS Nano* **2015**, *9*, 8869; f) Z. B. Sun, H. H. Xie, S. Y. Tang, X. F. Yu, Z. N. Guo, J. D. Shao, H. Zhang, H. Huang, H. Y. Wang, P. K. Chu, *Angew. Chem. Int. Ed.* **2015**, *54*, 11526; g) W. C. Zhao, Z. M. Xue, J. F. Wang, J. Y. Jiang, X. H. Zhao, T. C. Mu, *ACS. Appl. Mater. Interfaces* **2015**, *7*, 27608; h) H. U. Lee, S. Y. Park, S. C. Lee, S. Choi, S. Seo, H. Kim, J. Won, K. Choi, K. S. Kang, H. G. Park, H. S. Kim, H. R. An, K. H. Jeong, Y. C. Lee, J. Lee, *Small* **2016**, *12*, 214.
[9] S. Ge, L. Zhang, P. Wang, Y. Fang, *Sci. Rep.* **2016**, *6*, 27307.
[10] A. Castellanos-Gomez, M. Buscema, R. Molenaar, V. Singh, L. Janssen, H. S. J. van der Zant, G. A. Steele, *2D Mater.* **2014**, *1*, 1.
[11] Y. Zhao, H. Wang, H. Huang, Q. Xiao, Y. Xu, Z. Guo, H. Xie, J. Shao, Z. Sun, W. Han, X. F. Yu, P. Li, P. K. Chu, *Angew. Chem. Int. Ed.* **2016**, *55*, 5003.
[12] G. Ku, X. D. Wang, G. Stoica, L. H. V. Wang, *Phys. Med. Biol.* **2004**, *49*, 1329.
[13] K. Tokita, T. Katsuno, S. J. Hocart, D. H. Coy, M. Llinares, J. Martinez, R. T. Jensen, *J. Biol. Chem.* **2001**, *276*, 36652.
[14] a) S. E. A. Gratton, P. A. Ropp, P. D. Pohlhaus, J. C. Luft, V. J. Madden, M. E. Napier, J. M. DeSimone, *Proc. Natl. Acad. Sci. USA* **2008**, *105*, 11613; b) M. X. Yu, J. Zheng, *ACS Nano* **2015**, *9*, 6655.
[15] a) A. Kundu, S. Nandi, P. Das, A. K. Nandi, *J. Colloid Interface Sci.* **2016**, *468*, 276; b) Y. He, Y. L. Zhong, F. Peng, X. P. Wei, Y. Y. Su, S. Su, W. Gu, L. S. Liao, S. T. Lee, *Angew. Chem. Int. Ed.* **2011**, *50*, 3080.
[16] a) I. Lynch, K. A. Dawson, *Nano Today* **2008**, *3*, 40; b) E. C. Cho, Q. Zhang, Y. N. Xia, *Nat. Nanotechnol.* **2011**, *6*, 385.

Received: August 30, 2016
Revised: November 20, 2016
Published online: January 6, 2017

